Archives available at journals.mriindia.com

International Journal on Advanced Computer Engineering and Communication Technology

ISSN: 2278-5140

Volume 15 Issue 01, 2026

Deep Learning Assisted Lung Cancer Screening for Early Detection

T. Krishnaswamy

Department of Electronics and Communication Engineering, Arunachala College of Engineering for Women, Vellichanthai, Tamilnadu, India

Peer Review Information

Submission: 18 April 2026
Revision: 13 May 2026
Acceptance: 25 May 2026

Keywords

Lung Cancer Detection, Deep Learning, Computed Tomography (CT), Positron Emission Tomography (PET), DenseNet-121, Convolutional Neural Network (CNN), Autoencoder, Swin Transformer, Medical Image Analysis, Early Cancer Diagnosis.

Abstract

The leading cause of the greatest cancer-related death rate worldwide is lung cancer (LC). The only way to improve a patient's chances of survival is to detect lung cancer early. Nevertheless, the current LC detection models require a significant amount of processing power. The complexity of the model's execution presents difficulties for healthcare facilities. So, to detect and diagnose LC, deep learning (DL)-based medical image analysis is proposed. It uses computed tomography (CT) and positron emission tomography (PET) images to detect early indications of LC. To get rid of the noise and artifacts, efficient picture preprocessing and method was used. The DenseNet-121 model was used to create a Convolutional Neural Network (CNN) model for feature extraction. Deep autoencoders were used to reduce the dimensionality of the features. The features were utilized to determine the different types of LC using the Swin Transformer, a deep learning classifier. Performance was assessed using the Lung-PET-CT-Dx dataset. The experimental results demonstrated that, with fewer parameters, the suggested model achieved an accuracy of 98.6. The suggested methodology can be used in real time to help doctors and radiologists identify LC early on.

Introduction

Lung cells, particularly those found in the epithelial lining of the bronchi, bronchioles, or alveoli, are the source of lung cancer. Delays in diagnosing a medical problem have an impact on treatment effectiveness and reduce the chance of long-term survival [1]. Small cell lung cancer (SCLC) and non-small cell lung cancer (NSCLC) are the two prevalent forms of LC. Lung squamous cell carcinoma (LUSC) and lung adenocarcinoma (LUAD) are the two subtypes of NSCLC that are typically distinguished

Improving patient outcomes depends on early LC identification and treatment using efficient screening techniques. Low-dose helical CT screening is more successful [2] in lowering mortality among high-risk individuals, according to the results of the National Lung Screening Trial

There have been significant advancements in the field of LC detection, including new methods and tools for improving early diagnosis and treatment effectiveness. Blood samples are examined using liquid biopsies to look for [3] cancer. Genetic abnormalities and changes linked to LC can be detected by these diagnostic techniques. As a result, these tests provide a non-invasive way to identify the illness and track how well a treatment is working. A popular technique for the prompt detection of LC is low-dose computed [4] tomography (LDCT) screening. While providing high-resolution images of the pulmonary region, LDCT scans use less radiation than traditional CT scans. By identifying the illness in its early stages, DL-based LC screening methods can lower mortality [5]. By identifying early or subtle signs of LC that people might miss, it can help reduce false negatives (FN). DL algorithms

can be used to integrate imaging modalities such as CT, magnetic resonance imaging (MRI), and PET to better understand the disease and help with diagnosis and treatment planning. The degree of disease metastasis is directly correlated with cancer stage. By automating [6] LC identification using DL approaches, radiologists and doctors may have less work to do. Automation has the potential to increase consistency and speed. Therefore, the authors want to use the DL approach to develop an affordable LC detection model. The following contributions are included in the study:

An LC detection model for recognizing the kind of LC with less computational resources; a DL model for extracting important characteristics from the PET/CT images; and a performance evaluation of the suggested LC model using cutting-edge methods.

The following is the structure of the planned study: The related work is presented in section 2. The suggested methodology for categorizing different forms of LC using PET/CT scans is presented in Section 3. Section 4 presents the findings of the experiment. Section 5 presents the conclusion.

Related Works

Lung cancer is the formation of malignant cells in the lungs. The rising incidence of cancer has led to an increase in both male and female mortality rates. Uncontrollably proliferating cells in the lungs are the cause of lung cancer. Although lung cancer cannot be prevented, its risk can be decreased. Therefore, the survival rate [7] of patients depends on the early identification of lung cancer. The amount of lung cancer cases is directly correlated with the number of chain smokers. Classification methods such Naive Bayes, SVM, Decision Tree, and Logistic Regression were used to analyze the lung cancer prediction. The code for the Lung-CLiP classification model [8] and comprehensive patient-level genomic features used as input for the Lung-CLiP model, including genome-wide somatic copy number alteration data and somatic mutation genotyping data with all the associated features taken into consideration in the Lung-CLiP model. Images from Computer Tomography (CT) scans [9] are used to identify, categorize, and assess the degree of malignancy in lung nodules. The U-Net design is used to segment the CT scan images. The 3D multipath VGG-like network proposed in this paper is tested on 3D cubes taken from the lung image. To determine the probability that a CT scan is malignant, the feature set is input into several classifiers, such as Random Forest and XGBoost, and the individual predictions [10] are combined. The accuracy attained on LIDC-IRDI is 84%, surpassing earlier attempts. The dependency on extensive annotated data, overfitting, excessive computational complexity, and interpretability are some of the constraints of the current efforts. Third, there is still much to learn about the stability of these models' performance when applied to real clinical datasets. This is a more significant problem that will significantly limit the actual use of these models in clinical practice. In order to address them, we create a novel Cancer Nexus Synergy (CanNS) that uses [11] Devilish Levy Optimization (DevLO) for fine-tuning parameters, Xception-LSTM GAN (XLG) CancerNet for classification, and A. Swin-Transformer UNet (SwiNet) Model for segmentation. It is still necessary to increase the precision of conventional lung cancer detection techniques, particularly in practical diagnostic situations. In this work, we assessed how well the Swin Transformer [12] model performed in lung cancer segmentation and classification. According to the results, the pre-trained Swin-B model outperformed ViT by 2.529% with a top-1 accuracy of 82.26% in the classification task. The Swin-S model outperformed other approaches in the segmentation mission in terms of mean Intersection over Union (mIoU).

Methodology

The Figure 1 shows the Frame work for early detection of Lung Cancer using deep learning Swin Transformer Classification. To make PET/CT scans more visible, an image preprocessing method is first applied. For feature extraction, the DenseNet-121 model is employed. To lower the amount of features, dimensionality reduction technique is used. Lastly, LC is detected using improved Swin Transformer deep learning Classifier.

1. Image Acquisition

The suggested LC detection model is expanded by using the PET and CT (Lung-PET-CT-Dx) dataset. Lung-PET-CT-Dx is a recently developed dataset that comprises 31,562 annotated images. The repository makes it accessible to the public. The photos were gathered in retrospect from several medical facilities and oncology institute. The dataset did not contain any personal information about the patient. CT and PET-CT DICOM pictures of LC patients are included in the dataset. It offers bounding boxes and XML annotation files that show the location of tumors. The patients were categorized based on the tissue histopathological diagnosis. The resolution of the CT and PET images was 512 × 512 pixels at 1 mm × 1 mm and 200 × 200 pixels

at 4.07 mm × 4.07 mm, respectively. The tumor location was annotated by five university thoracic radiologists with experience in LC identification. Adenocarcinoma (A), small cell carcinoma (B), big cell carcinoma (E), and squamous cell carcinoma are the general categories into which the photos were divided.

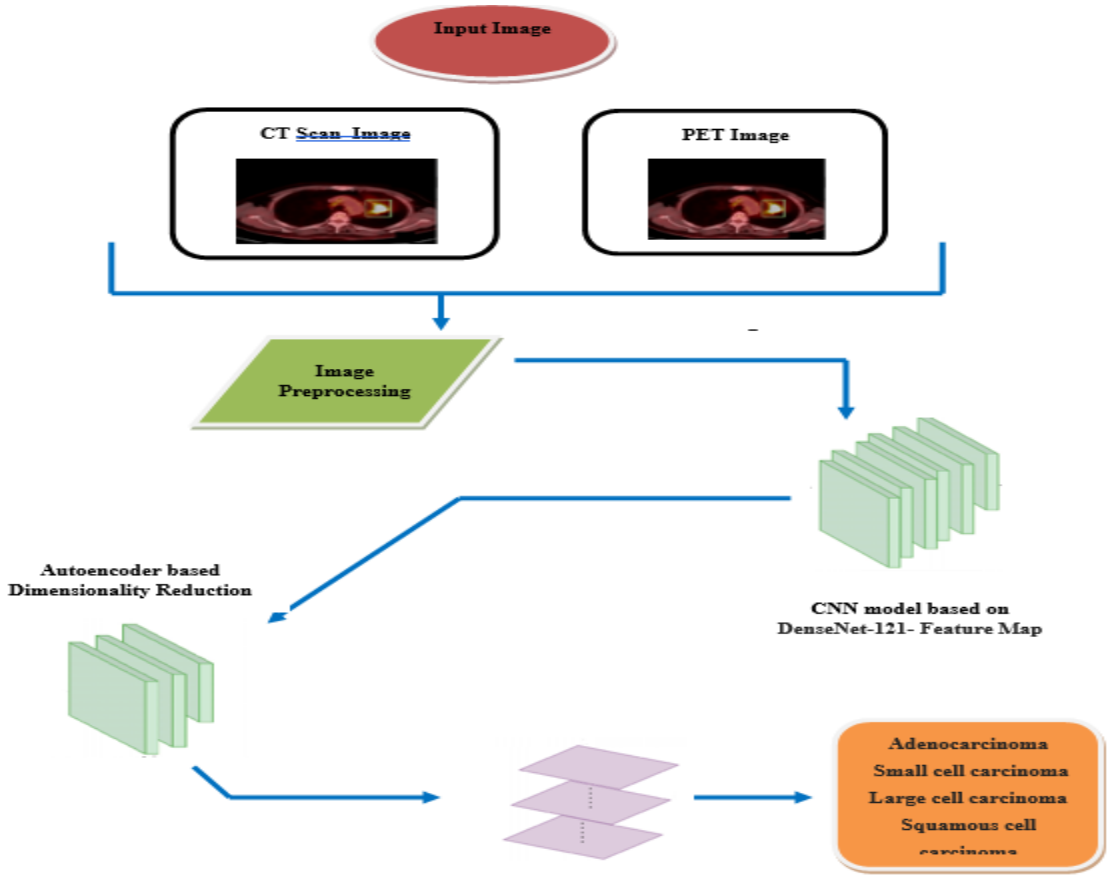

Figure1: Proposed Lung Cancer Detection Framework

2. Image preprocessing

Since PET and CT scans are typically acquired separately, patient motion may cause misalignment. These images may be affected by a variety of abnormalities, such as metal artifacts in CT scans and motion artifacts in PET scans. The purpose of picture registration is to ensure that two images are spatially aligned. For non-linear image registration, the symmetric normalization (SyN) function is frequently employed. To address the deformations and enhance the image alignment, the author used the SyN function. The SyN function combines CT anatomical information with PET metabolic activity.

Equation (1) illustrates how the SyN function is calculated. The function creates a Gaussian pyramid to represent the complex deformation in the PET/CT images. In order to produce the spatially coincident features, it determines the spatial transformation.

$$I = SyN(Ii, \varphi 1, \varphi 2), i = 1, 2, ..., n \quad (1)$$

Where, $\varphi 1$ and $\varphi 2$ velocities to normalize the pictures and cross-correlation are calculated using diffeomorphism variables

The spatial resolutions and voxel sizes of PET and CT images may differ. The resample image filter feature is used by the author to adjust the PET/CT images' spatial resolution. In order to produce a significant result, the resample image filter function supports the suggested model and standardizes the PET/CT picture dimensions.

$$Ii = Resample\_Image\_Filter(Ii, s, scale, NI), i = 1, 2, ..., n \quad (2)$$

Where,

NI - The nearest neighbor interpolation

Scale - The scaling factor

s - Image size.

The PET/CT images' anatomical and functional information is improved by the attenuation correction tool. By minimizing the artifact impressions, it reconstructs the images. By measuring the attenuation of the gamma ray photons, the attenuation correction function detects changes in tissue density. By creating

the principal photon attenuation, it lessens the effect of scatter artifacts. To lessen the metal artifacts, the metal attenuation correction algorithm uses an iterative reconstruction method. Additionally, it substitutes interpolated values of the surrounding tissue regions in the pictures for the metal artifact regions.

$$Ii = attenuation(Ii, A) + Metal\_attenuation(Ii, M),\ i = 1, 2, ..., n \quad (3)$$

Where,

A and M - The attenuation coefficients used to lessen the artifacts' effect.

Retinex filtering approach is used to handle non-uniform illumination and shading of PET/CT images in order to increase the contrast level of the image. The PET/CT images' color and brightness are improved using Retinex filtering. It keeps the images' features and general structure intact. It uses the lighting and reflectance components to break down the images.

$$Ii = Retinex\_Filter(Ii, IM, RF),\ i = 1, 2, ..., n \quad (4)$$

Where, RF stands for reflectance and IM for illumination.

3. Feature Extraction

The pre-trained DenseNet-121 model's weights are used by the author to construct a feature extraction model. The features are extracted using a series of convolutional layers, batch normalization, and the ReLu function. The DenseNet-121 model's weight is used to train the last set of layers in the feature extraction model at a learning rate of 1 × 10−3. Feature extraction using the frozen pre-trained DenseNet-121 model requires less parameters. Ultimately, each image's fixed-size feature vector is obtained by the global average pooling layer. The computational resources needed to classify the PET/CT images are reduced by the feature extraction procedure. The mathematical forms of producing fixed-size features are presented in equations (6) and (7).

$$Features=Convolution+ReLu+Batch\_Normalization(Ii),\ i=1,\ldots,n \quad (5)$$

$$Fixed\_size\_features=Global\_Average\_Pooling\_2D(features) \quad (6)$$

4. Dimensionality Reduction

By creating a compact latent space representation, deep autoencoders reduce the dimensionality of PET/CT images. The frame work is shown in Figure 2. This technique attempts to rebuild the input image from its compressed lower-dimensional representation using encoder–decoder architecture. To lower the dimensionality of the features, the author employs a multilayer encoder network. By using learned weights and biases, the encoder's layers enable the transformation of input data into an expression of reduced dimensionality. Convolutions, pooling, and non-linear activations are some of the methods used to reduce dimensions.

The latent space is the limiting factor in the autoencoder design. The input image's basic components and patterns are captured in the condensed form. The decoder network tries to replicate the original feature using the low-dimensional representation from the latent space. Decoder layers increase the representation's number of dimensions. The constriction in the latent space is responsible for the reduction in dimensionality. The encoder network eliminates extraneous or similar data while maintaining the features' important qualities.

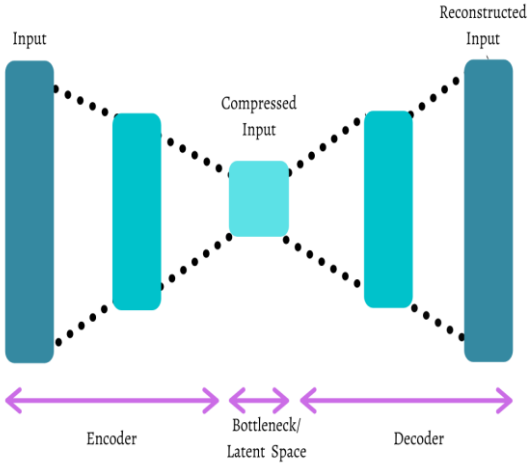

Figure 2 Frame work for Dimensionality Reduction Autoencoders

5. Lung Cancer (LC) Detection

The auto encoder's 256-dimensional compressed feature vector is fed into the Swin-Tiny backbone of the LC Classification model shown in Figure 3, which is based on the Swin Transformer block. Since the input is already small, the initial patch embedding is skipped. It uses shifted window attention on 16*16*192 tokens to simulate the fine nodule boundary connections that differentiate squamous cell carcinoma from adenocarcinoma, such as lobulation and smoothness. It then combines patches into 8*8*384 and use attention to catch micro-level phenomena like cavitation and speculation. The model may relate overall form to malignancy subtype in the next step, which decreases to 4*4*768 where each token can attend globally over the entire nodule. This is crucial for distinguishing between Small Cell Carcinoma, which lacks spicules, and Large Cell Carcinoma. The 4*4*768-D vector that encodes both local texture and global morphology is

collapsed by global average pooling following the transformer phases. The final probabilities for adenocarcinoma, small cell carcinoma, large cell carcinoma, and squamous cell carcinoma are obtained by passing this vector through a classification head. Swin's shifted window mechanism explicitly connects features across the nodule, in contrast to other deep learning classification methods that rely on 3*3 convolutions. This means that a spicule on one edge can affect the prediction along with texture on the opposite edge, making it much stronger for subtypes where global shape and long-range patterns matter.

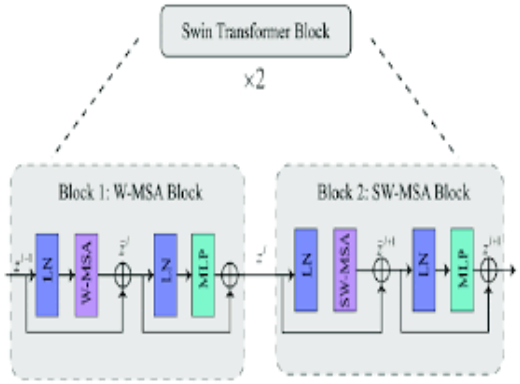

Figure 3: Swin Transformer

In order for the model to learn fine-grained texture patterns, such as the ground glass opacity characteristic of Adenocarcinoma, the W-MSA part divides the nodule feature map into local windows and computes attention within each. The SW-MSA part then shifts those windows, allowing attention to cross the previous boundaries and connect distant features, which is crucial for capturing long-range speculation and irregular borders that distinguish Squamous Cell Carcinoma from Small Call Carcinoma.

6. Performance metrics

True positives (TPs), true negatives (TNs), FPs, and FNs all have distinct meanings in the context of LC detection. A TP denotes a particular LC type that has been correctly identified, TN denotes an image that has been successfully identified but belongs to a different LC type, FP denotes an LC type that has been incorrectly identified, and FN denotes an image that has been incorrectly identified but belongs to a different LC type. The accuracy metric evaluates the suggested model's prediction quality. It calculates the percentage of correctly predicted instances (including TP and TN) relative to the total number of instances in the dataset. The percentage of instances where the model produced an optimistic prediction is known as precision. The percentage of TP predictions among all positive cases is known as recall. The precision and recall harmonic mean is displayed by the F1-score. A model that continuously demonstrates strong recall and precision levels is indicated by a higher F1-score. For the LC detection models, AU-ROC, the precision–recall curve (AU-PRC), and the loss function are also calculated.

$$Accuracy=TP+TNTP+TN+FP+FN \quad (7)$$

$$Precision=TPTP+FP \quad (8)$$

$$Recall=TPTP+FN \quad (9)$$

$$F1-Score=2\times Precision\times Recall(Precision+Recall) \quad (10)$$

Result and Discussion

The experiment is conducted in python 3.8.3 and the following Figure 4 shows the input and the preprocessed images

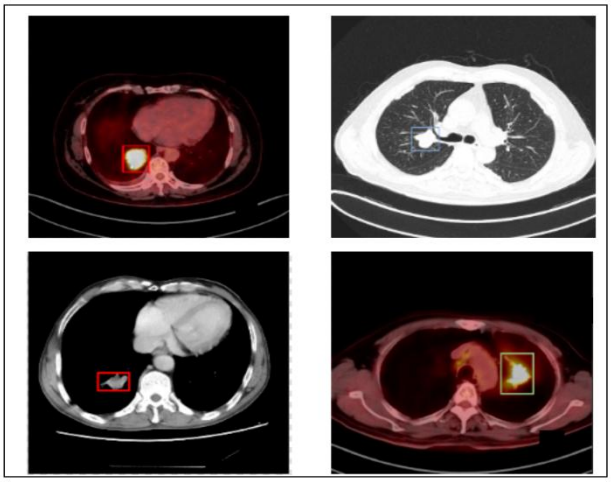

(a) Sample LC CT and PET Image

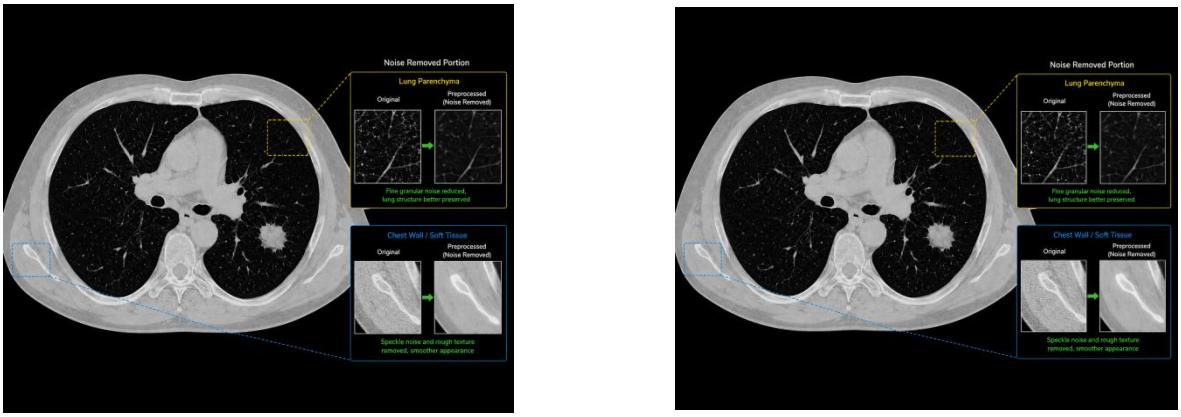

(b) Noise Removed CT and PET LC Images

Figure 4: (a) Sample LC CT and PET Images (b) Noise Removed CT and Pet

Figure 4 (a) shows raw sample LC CT and PET images with obvious noise and artifacts that can confound during feature extraction. Lung boundaries, nodule edges, and PET uptake regions are crisper and cleaner in Figure 4 (b), which shows the same slices after noise removal.

The results of the CNN model based on DenseNet-121's feature extraction process are displayed in Figures 5 (a) and (b). By the final 7*7 Final Features, the DenseNet has eliminated background noise and retained only the crucial cancer-related hints. The model focuses on the tumor region in both CT and PET images, as indicated by the yellow bright spot.

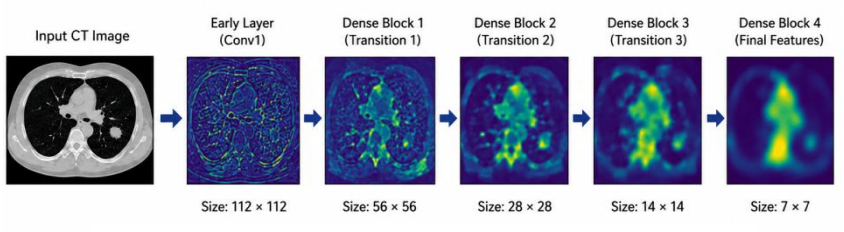

(a) Feature Map of Input CT Image

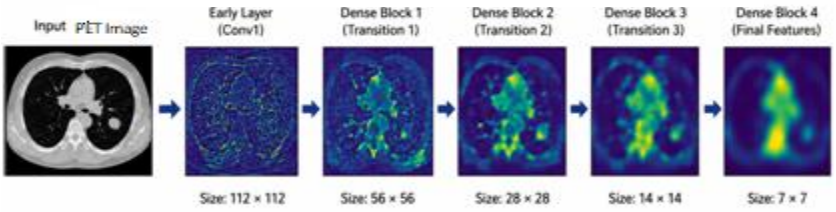

(b) Feature Map of Input PET Image

Figure 5 (a) and (b) Extracted Feature Map using CNN model based on DenseNet-121

The Swin Transformer classification's performance metrics are listed in Table 1. The Swin Transformer uses autoencoder features and global context acquired by DenseNet-121 to conduct classification. The suggested model's 98% accuracy indicates that its performance is dependable. Simply put, the suggested deep learning swin model is far more powerful than previous models and can accurately identify the cancer subtypes.

Table 1. Findings of the Performance Metrics of the Swin Transformer Classification

Types of LC	Accuracy (%)	Precision (%)	Recall (%)	F1 Score (%)
Adenocarcinoma	98.5	98.1	98.3	96.5
Small Cell Carcinoma	98.3	98.5	98.6	96.4
Large Cell Carcinoma	98.6	97.4	97.2	95.4
Squamous Cell Carcinoma	98.4	97.8	97.9	95.3

Conclusion

This work introduces a deep learning system for early lung cancer detection that analyzes CT and PET images using DenseNet-121, deep autoencoders, and Swin Transformer. The suggested model efficiently lowers noise through preprocessing, uses CNN-based DenseNet-121 to extract robust features, compresses them using autoencoders, and uses Swin Transformer's shifted window attention to classify LC. The model performed well in differentiating between adenocarcinoma, small cell, large call, and squamous cell carcinoma, with an accuracy of 98.6%.The system's dependability is confirmed by the excellent precision, recall, and F1. This methodology provides a useful option for healthcare institutions and can help radiologists diagnose early-stage lung cancer accurately due to its lightweight design and real-time capacity.

Reference

Inage, T., Nakajima, T., Yoshino, I., & Yasufuku, K. (2018). Early lung cancer detection. Clinics in Chest Medicine, 39(1), 45–55.

Asuntha, A., & Srinivasan, A. (2020). Deep learning for lung cancer detection and classification. Multimedia Tools and Applications, 79(11), 7731–7762.

Günaydin, Ö., Günay, M., & Şengel, Ö. (2019). Comparison of lung cancer detection algorithms. In 2019 Scientific Meeting on Electrical-Electronics & Biomedical Engineering and Computer Science (EBBT) (pp. 1–4). IEEE.

Makaju, S., Prasad, P. W. C., Alsadoon, A., Singh, A. K., & Elchouemi, A. (2018). Lung cancer detection using CT scan images. Procedia Computer Science, 125, 107–114.

Javed, R., Abbas, T., Khan, A. H., Daud, A., Bukhari, A., & Alharbey, R. (2024). Deep learning for lungs cancer detection: A review. Artificial Intelligence Review, 57(8), 197.

Gayap, H. T., & Akhloufi, M. A. (2024). Deep machine learning for medical diagnosis, application to lung cancer detection: A review. BioMedInformatics, 4(1), 236–284.

Radhika, P. R., Nair, R. A. S., & Veena, G. (2019). A comparative study of lung cancer detection using machine learning algorithms. In 2019 IEEE International Conference on Electrical, Computer and Communication Technologies (ICECCT) (pp. 1–4). IEEE.

Chabon, J. J., Hamilton, E. G., Kurtz, D. M., Esfahani, M. S., Moding, E. J., Stehr, H., Schroers-Martin, J., et al. (2020). Integrating genomic features for non-invasive early lung cancer detection. Nature, 580(7802), 245–251.

Tekade, R., & Rajeswari, K. (2018). Lung cancer detection and classification using deep learning. In 2018 Fourth International Conference on Computing Communication Control and Automation (ICCUBEA) (pp. 1–5). IEEE.

Bhatia, S., Sinha, Y., & Goel, L. (2018). Lung cancer detection: A deep learning approach. In Soft Computing for Problem Solving: SocProS 2017, Volume 2 (pp. 699–705). Springer Singapore.

Durgam, R., Panduri, B., Balaji, V., Khadidos, A. O., Khadidos, A. O., & Selvarajan, S. (2025). Enhancing lung cancer detection through integrated deep learning and transformer models. Scientific Reports, 15(1), 15614.

Sun, R., Pang, Y., & Li, W. (2023). Efficient lung cancer image classification and segmentation algorithm based on an improved Swin Transformer. Electronics, 12(4), 1024.